26. A. Rochon, A. de Vernal, H. P. Sejrup, H. Haflidason, *Quat. Res.* **49**, 197 (1998).
27. J. N. Deo, J. O. Stone, J. K. Stein, *Am. Antiq.* **69**, 771 (2004).
28. W. S. Cleveland, *The Elements of Graphing Data* (AT&T Bell Laboratories, Murray Hill, NJ, 1994).
29. We acknowledge comments from B. F. Atwater and B. Kromer and four anonymous reviewers that helped to improve the manuscript. The work was supported by the Norwegian Research Council and the University of Tromsø. Ø. S. Lohne and D. Bondevik participated in the field, G. Skjerdal picked plant fragments, and P. J. Svanem and S. Stene combusted the samples to graphite. J.M. conceived the project, S.B. did the fieldwork and led the laboratory work and writing, H.B. identified plant fragments, S.G. conducted the radiocarbon dating, and P.R. ran the marine box model.

Supporting Online Material
www.sciencemag.org/cgi/content/full/312/5779/1514/DC1
Materials and Methods
Figs. S1 and S2
Tables S1 and S2
References

1 December 2005; accepted 28 April 2006
10.1126/science.1123300

Transatlantic Abundance of the N_2-Fixing Colonial Cyanobacterium *Trichodesmium*

Cabell S. Davis[1]* and Dennis J. McGillicuddy Jr.[2]

Colonial diazotrophic cyanobacteria of the genus *Trichodesmium* are thought to play a significant role in the input of new nitrogen to upper layers of the tropical and subtropical oceanic ecosystems that cover nearly half of Earth's surface. Here we describe results of a transatlantic survey in which a noninvasive underwater digital microscope (the video plankton recorder), was towed across the North Atlantic at 6 meters per second while undulating between the surface and 130 meters. Colony abundance had a basin-scale trend, a clear association with anticyclonic eddies, and was not affected by hurricane-forced mixing. Subsurface abundance was higher than previously reported, which has important implications for the global ocean nitrogen cycle.

Tropical and subtropical regions of the ocean represent the largest ecosystems on Earth, covering nearly half the planet's surface. This vast oligotrophic area has been termed a biological desert because of low observed nutrient concentrations and biomass (*1*), but it is important in global carbon cycling due to biological feedbacks including surface heating and gas exchange and the sinking export of fixed carbon from the surface layer via the biological pump (*2*, *3*). Production in these regions is nitrogen limited, and carbon and nitrogen cycles cannot be balanced by traditional mechanisms of nitrate supply, such as are derived from winter mixing and vertical diffusion (*4*). Data and modeling indicate that episodic upwelling of deep nitrogen-rich water by mesoscale eddies is a potentially important but undersampled mechanism for input of new nitrogen into the biologically active upper layer of the oligotrophic ocean (*5*). Another potentially important source of new nitrogen is from N_2 fixation by diazotrophic colonial cyanobacteria of the genus *Trichodesmium*, which are ubiquitous members of tropical and subtropical pelagic communities (*6*–*12*). Globally, *Trichodesmium* has been estimated to generate 80 to 110 Tg of new nitrogen per year in oligotrophic waters, accounting for a significant proportion of the annual input of new nitrogen (*6*, *11*–*15*). It is considered the dominant N_2 fixer in the tropical-subtropical ocean (*16*). Mechanisms controlling abundance of *Trichodesmium* have been extensively studied, with iron and/or phosphorus limitation thought to play a major role (*17*). *Trichodesmium* abundance has been difficult to quantify using traditional net sampling, because the colonies are easily damaged or destroyed during collection, which results in underestimation (*18*, *19*). Sampling with bottles (e.g., 10-liter Niskin) has provided quantitative estimates of vertical abundance over broad areas of the tropical Atlantic (*18*), whereas current estimates of abundance in the Sargasso Sea are based largely on net tows.

We used an in situ digital microscope to quantify the abundance of *Trichodesmium* noninvasively across the Sargasso Sea during August and September 2003. We towed the video plankton recorder (VPR) (*20*–*23*) from the Azores toward Bermuda, continuing across the Gulf Stream to the Slope Water south of Cape Cod, Massachusetts (Fig. 1A). This sampling was done opportunistically during a transit leg of the R/V *Knorr* and was carried out at the cruising speed of the ship (6 m/s) over a 12-day period, covering a distance of 5517 km. The VPR undulated automatically between the surface and 130 m below with an average vertical velocity of 1 m/s, yielding a total of 6910 vertical profiles. The ship's track was intentionally diverted to intersect cyclonic and anticyclonic mesoscale ocean eddies during the transit (Fig. 1B). Eddy positions were determined by shore-based analysis of near-real-time satellite sea-surface altimetry data and sent to the ship by e-mail (*23*). East of Bermuda, the ship's track was diverted to the southwest to avoid a category 3 hurricane (*Fabian*). As *Fabian* crossed Bermuda, the ship turned northwest toward Woods Hole, and sampling continued across the wake of the storm (Fig. 1, A and B).

[1]Biology Department, Woods Hole Oceanographic Institution, [2]Department of Applied Ocean Physics and Engineering, Woods Hole Oceanographic Institution, Woods Hole, MA 02543–1541, USA.

*To whom correspondence should be addressed. E-mail: cdavis@whoi.edu

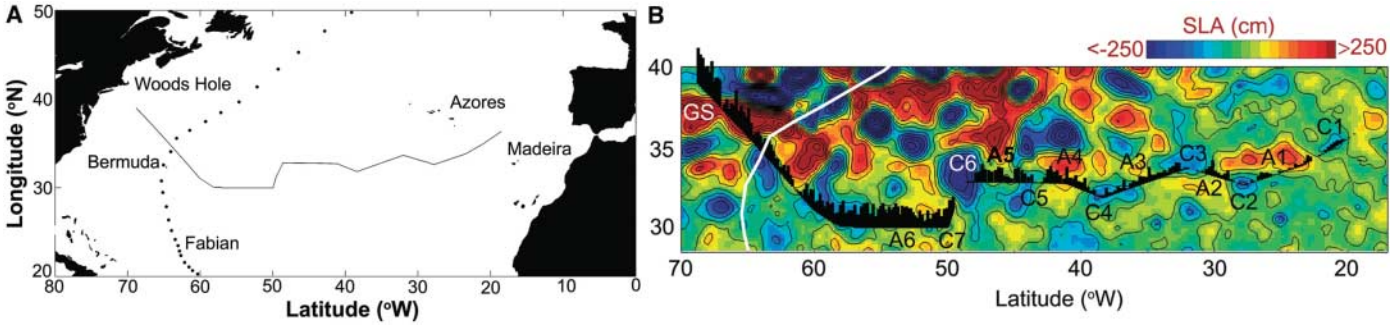

Fig. 1. (**A**) Cruise track of the R/V *Knorr* across the North Atlantic from the Azores to the Slope Water south of Woods Hole, Mass. (28 August to 8 September 2003). Dots show 3-hour positions of hurricane Fabian. (**B**) Along-track histogram of hourly *Trichodesmium* abundance (number/m^3) (puffs) (Fig. 2A top panel) overlaid on a contour plot of sea surface height (sea level anomaly, SLA) from satellite altimetry data on 3 September 2003. Highs and lows in the SLA data are labeled to show positions of seven cyclonic (C) and six anticyclonic (A) eddies as well as the Gulf Stream (GS). Note lower *Trichodesmium* abundance in cyclonic eddies on the eastern half of transect. White line is path of hurricane Fabian.

The VPR is equipped with a 1-megapixel digital video camera sampling 30 frames per second. The lens was adjusted to give a field of view of 1.2 cm, and the calibrated imaged-volume was 11.88 ml. Average spacing between adjacent images was 3.3 cm vertically (20 cm horizontally), and the total volume sampled was 356 ml per vertical meter or 46 liters per 130-m profile. The VPR also had sensors for conductivity, temperature, pressure, fluorescence, turbidity, and photosynthetically active radiation. Raw sensor data were logged at 30 Hz, and 1-s averages were logged together with global positioning system (GPS) latitude, longitude, Greenwich mean time (GMT) at 1 Hz. Images of plankton were sorted automatically into different taxa by using classifiers trained with a set of manually sorted images.

The automatically sorted *Trichodesmium* images were examined manually to remove false-positives (*23*). The list of observation times for *Trichodesmium* images were binned into the 1-s time bins of the sensor and GPS data, and the number in each bin was divided by the total volume imaged during each 1-s period to give the average abundance (number/m^3) per bin. These values then were divided by the probability of detection to provide accurate abundance estimates (*21*, *23*). In addition to the binned data, the latitude, longitude, and depth associated with each individual *Trichodesmium* image was determined, by using interpolation, from image acquisition time and GPS time. Only colonies were readily identified from the VPR images, with free trichomes difficult to distinguish from other taxa (e.g., diatom chains) at the magnification used. So abundances presented here are underestimates of total trichome concentration, although free trichomes on average typically represent ~10% of the total (*18*).

We found strong signals in temperature, salinity, and abundance of *Trichodesmium* colonies corresponding to seven cyclonic and six anticyclonic eddies and the Gulf Stream (Fig. 2A). Vertical distributions of temperature and salinity revealed strong subsurface signatures in the eddies observed via satellite altimetry. Likewise, the acoustic Doppler current profiler mounted on the hull clearly revealed the circulation patterns in these eddies (fig. S3).

Trichodesmium images, sorted into two morphological classes, puffs and tufts, were likely *T. thiebautii*, with the tufts also including *T. erythraeum* (*24*, *25*). Both forms had basin-scale trends in abundance, with higher concentrations in the western Sargasso Sea (west of 50°W) (Figs. 1B and 2A). Mean colony abundances (both forms combined) were 35.1 ± 2.8 m^{-3} and 6.4 ± 0.7 m^{-3} (±2 SEM) in western and eastern regions, respectively. An association of *Trichodesmium* with warm salty water was evident at the eddy scale, with relatively higher concentrations found in warm anticyclonic eddies than

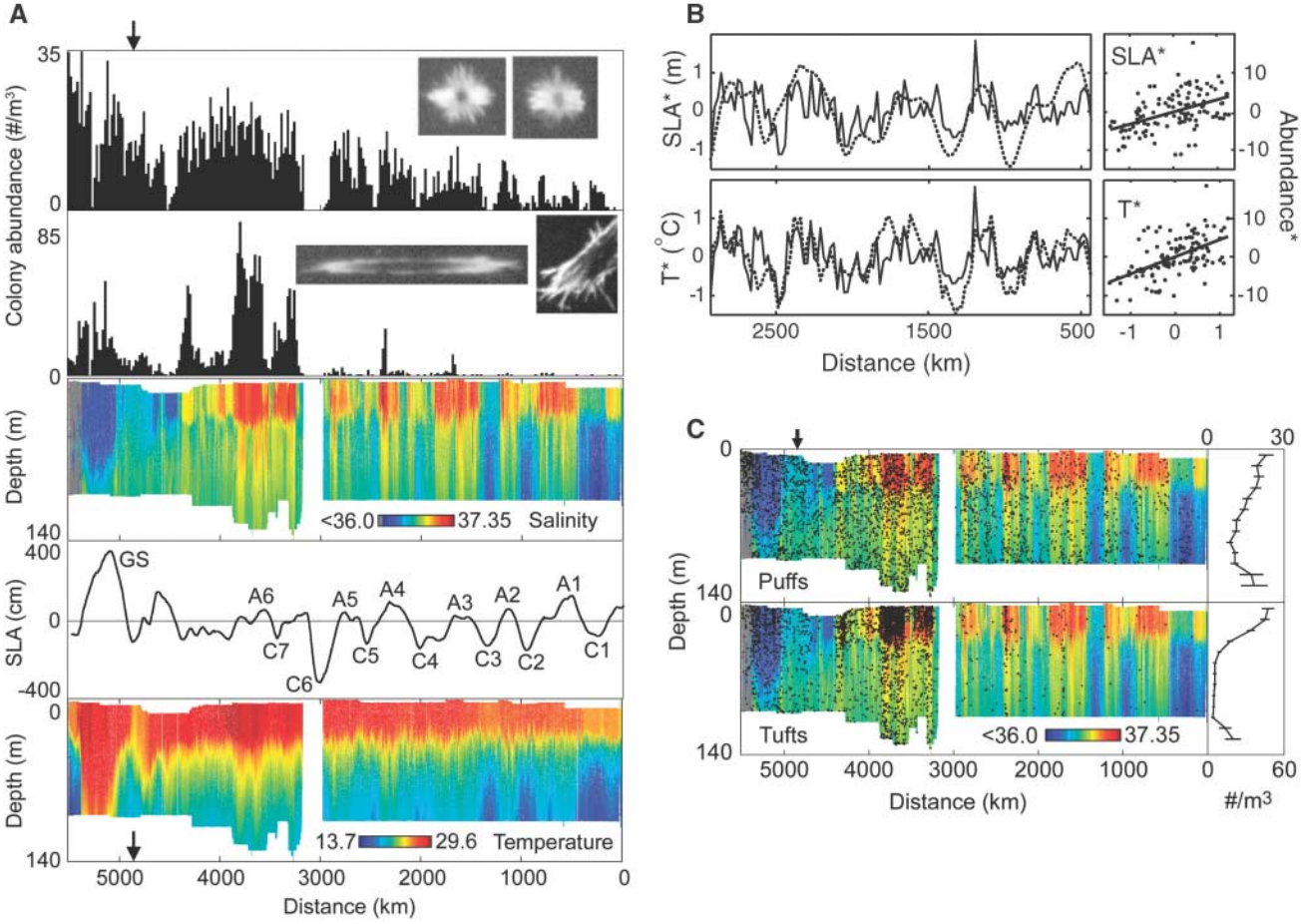

Fig. 2. (**A**) Hourly mean abundance (number/m^3) of *Trichodesmium* colonies across the Atlantic Ocean. VPR images of spherical (puffs) and fusiform (tufts) are shown in the top and second panels, respectively (image widths, 1 to 3 mm). Salinity, along-track SLA, and temperature are shown below. Data points for salinity and temperature are 1-s averages and abut each other in the plots. Cyclonic and anticyclonic eddies and the Gulf Stream are labeled as in Fig. 1B. Arrows indicate the point of intersection with the wake of hurricane *Fabian*. (Data gap is due to removal of VPR from water during hurricane avoidance maneuver.) (**B**) (Left) Detrended hourly SLA (SLA*, dotted curve), temperature (T*, dotted curve), and abundance (abundance*, solid curves) versus distance along the initial 500- to 3000-km portion of the transect. (Right) Linear regressions of Abundance* on SLA* and T* ($P < 0.0001$). (**C**) Vertical distributions of *Trichodesmium* puffs and tufts overlaid on salinity sections. Dots indicate locations of individual colonies. The mean vertical distributions across the entire transect are shown at right (error bars, 95% confidence intervals of hourly mean abundance at each depth). Arrow (top) shows intersection of hurricane *Fabian*'s wake.

in cold cyclonic eddies (Figs. 1B and 2A). This relation is especially evident for puffs during the 500- to 3000-km portion of the transect, where their abundance closely followed the sea level anomaly and temperature variability ($P < 0.0001$) (Fig. 2B). [An exception to this relation is the subsurface maximum of puff abundance in cyclone C1 (Fig. 1B).] The mechanisms responsible for higher abundance of *Trichodesmium* in anticyclonic eddies are unknown. This covariance could reflect eddy-driven transport of these populations from a distant source region. Alternatively, biotic interactions may be the controlling factor. The last-mentioned aspect is particularly enigmatic given the traditional paradigm that nitrogen fixation is generally phosphorus limited (*26*): Depression in the seasonal thermocline in these anticyclones (Fig. 2A) would tend to deepen the phosphocline and thereby reduce the availability of phosphorus in the eddy cores.

Although the relatively fragile colonies of *Trichodesmium* can be destroyed when wind mixing is strong (*27*), we did not find any indication of lower colony abundance across the wake of hurricane *Fabian*, despite maximum sustained winds of 200 km hr^{-1} (Fig. 2A). Mean colony concentration in the 200-km-wide wake region (23.0 ± 3.8 m^{-3}) was not significantly different from that in adjacent (200 km) areas (26.6 ± 7.0 m^{-3}, $P = 0.53$). It appears that both puff and tuft colonies were able to withstand this strong wind forcing.

Vertically, both forms were found throughout the water column (Fig. 2C) and were not restricted to the near surface as previously found in this area from net tows (*8*, *24*, *25*, *28*). Tufts were more abundant in the upper 50 m, especially in the warmest saltiest layer, yet abundance of puffs was high at all depths. Comparing these vertical distributions with ones derived from an empirical equation describing colony abundance versus depth in this region (*24*), as well as with earlier data from the Sargasso Sea (fig. S3), reveals that the abundances observed using nondestructive optical sampling are much higher at these depths than previously reported (Fig. 3 and fig. S4). This difference may be because deep net tows allow more time for fragile colonies to fragment (*19*) (with resulting trichomes extruded through net mesh openings), whereas shorter surface collections may be less destructive. By contrast, high abundance of trichomes at depths to 100 m have been found from quantitative bottle collections in the tropical North Atlantic during June under windy conditions, although overall abundance decreased markedly with depth (*18*).

We examined the potential impact of our abundance measurements on estimation of *Trichodesmium* nitrogen fixation in the water column, using published data on nitrogen fixation rates. The rate at a given depth was computed from the product of colony abundance and nitrogen fixation rate per colony, the latter being a function of light level, which decreases exponentially with depth. The rate per colony was estimated from linear and nonlinear empirically derived light-dependent functions on the basis of two separate data sets (*23*) (figs. S1 and S2).

Using VPR abundance data together with the nonlinear equation for light-dependent nitrogen fixation (*23*), we found the basin-scale average nitrogen fixation rate to be 2.7 to 5.0 times that expected from net-based sampling (Fig. 3A). Although the linear model gave lower overall rates, the VPR-based values were 2.9 to 3.3 times the net-based rates (table S1). The nitrogen fixation rate computed for the western Sargasso Sea (3250 to 3850 km) (50.54 μmol $N \cdot m^{-2} \cdot d^{-1}$) was three times that of the basin-scale average from the entire transect (16.74 μmol $N \cdot m^{-2} \cdot d^{-1}$) (Fig. 3B). Colony abundances in this region, however, are typically lower (e.g., 50 m^{-3}) than in tropical regions (e.g., 1000 m^{-3}) (*17*, *18*, *26*, *29*). If traditional net sampling methods have systematically underestimated deep colony abundance in other ocean regions, we can expect a substantial increase in the global *Trichodesmium* nitrogen fixation rate based on those studies. Such an increase could potentially account for the missing nitrogen in the global geochemical nitrogen cycle and could make this genus a crucial component to the productivity of the world ocean (*17*). Measurements made from bottle casts in the tropical Atlantic also reveal high abundance of *Trichodesmium* at these depths at certain times of year (*18*). Limited horizontal resolution of station sampling, however, may undersample the characteristically patchy distribution of *Trichodesmium* (*30*).

Further field and modeling studies are needed to determine the physical, chemical, and biological interactions controlling the multiscale distribution of *Trichodesmium*. The patchy nature of this species causes a large uncertainty in its population estimates (and thus in its role in oceanic N_2 fixation), and high-resolution large-scale sampling is required for quantitative assessment of its abundance and biomass (*17*). Satellite remote sensing is a promising new tool for quantifying surface distributions of *Trichodesmium* biomass (*30*), but this method does not quantify its vertical distribution. Nondestructive sampling, such as in situ optical imaging, is needed for determining the extent of its vertical distribution in other regions of the world ocean.

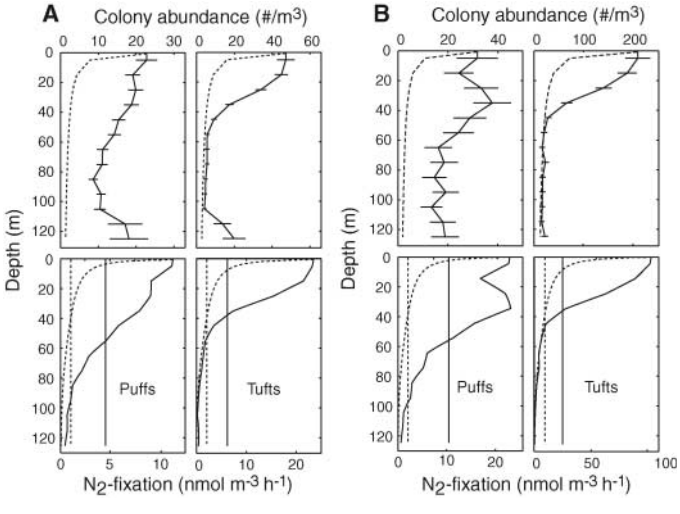

Fig. 3. (**A**) Vertical distribution of *Trichodesmium* puff (left) and tuft (right) abundance (top) and computed (light-dependent) N_2 fixation rates (bottom). Dashed curves are net-based estimates (see fig. S3 for data points) and solid curves are VPR-based. Curves in bottom panels are the corresponding N_2 fixation rates derived using the nonlinear function of N_2 fixation versus light (*23*). Straight lines in bottom panels are water column averaged N_2 fixation rates; VPR-based estimates are 2.7 to 5.0 times as high as net-based rates. (**B**) As in (A), except for the high-abundance region (3250 to 3850 km) only.

References and Notes

1. J. H. Ryther, *Science* **166**, 72 (1969).
2. S. Sathyendranath, A. D. Gouveia, S. R. Shetye, P. Ravindran, T. Platt, *Nature* **349**, 54 (1991).
3. P. Falkowski *et al.*, *Science* **290**, 291 (2000).
4. W. J. Jenkins, *Nature* **331**, 521 (1988).
5. D. J. McGillicuddy *et al.*, *Nature* **394**, 263 (1998).
6. D. G. Capone, J. P. Zehr, H. W. Paerl, B. Bergman, E. J. Carpenter, *Science* **276**, 1221 (1997).
7. D. G. Capone *et al.*, *Mar. Ecol. Prog. Ser.* **172**, 281 (1998).
8. E. J. Carpenter, C. C. Price, *Limnol. Oceanogr.* **22**, 60 (1977).
9. E. J. Carpenter, in *Nitrogen in the Marine Environment*, E. J. Carpenter, D. G. Capone, Eds. (Academic Press, New York, 1983), pp. 65–103.
10. E. J. Carpenter, K. Romans, *Science* **254**, 1356 (1991).
11. E. J. Carpenter, T. Roenneberg, *Mar. Ecol. Prog. Ser.* **118**, 267 (1995).
12. D. M. Karl *et al.*, *Biogeochemistry* **57/58**, 47 (2002).
13. V. J. Coles, R. R. Hood, M. Pascual, D. G. Capone, *J. Geophys. Res. Oceans* **109**, 1 (2004).
14. P. G. Falkowski, R. T. Barber, V. Smetacek, *Science* **281**, 200 (1998).
15. R. R. Hood, V. J. Coles, D. G. Capone, *J. Geophys. Res. Oceans* **109**, 1 (2004).
16. L. I. Falcon, E. J. Carpenter, F. Cipriano, B. Bergman, D. G. Capone, *Appl. Environ. Microbiol.* **70**, 765 (2004).
17. D. G. Capone *et al.*, *Global Biogeochem. Cycles* **19**, 1 (2005).
18. E. J. Carpenter, A. Subramaniam, D. G. Capone, *Deep–Sea Res. I* **51**, 173 (2004).
19. J. Chang, *J. Exp. Mar. Biol. Ecol.* **245**, 212 (2000).
20. C. S. Davis, S. M. Gallager, A. R. Solow, *Science* **257**, 230 (1992).
21. C. S. Davis, Q. Hu, S. M. Gallager, X. Tang, C. A. Ashjian, *Mar. Ecol. Prog. Ser.* **284**, 77 (2004).
22. C. S. Davis, F. T. Thwaites, S. M. Gallager, Q. Hu, *Limnol. Oceanogr. Methods* **3**, 59 (2005).
23. Additional materials and methods are given as supporting material on *Science* Online.

24. K. M. Orcutt *et al.*, *Deep–Sea Res. II* **48**, 1583 (2001).
25. J. J. McCarthy, E. J. Carpenter, *J. Phycol.* **15**, 75 (1979).
26. T. Tyrrell *et al.*, *J. Plankton Res.* **25**, 405 (2003).
27. E. J. Carpenter, C. C. Price, *Science* **191**, 1278 (1976).
28. E. J. Carpenter, J. J. McCarthy, *Limnol. Oceanogr.* **20**, 389 (1975).
29. A. F. Post *et al.*, *Mar. Ecol. Prog. Ser.* **239**, 241 (2002).
30. R. R. Hood, A. Subramaniam, L. R. May, E. J. Carpenter, D. G. Capone, *Deep–Sea Res. II* **49**, 123 (2002).
31. We thank the officers and crew of the R/V *Knorr* for their outstanding support during the transatlantic VPR sampling. B. Walden provided facilities support for use of the VPR. F. Thwaites, A. Girard, and M. Alberico assisted in system deployment and operations. V. Kosnyrev provided daily altimetry maps and eddy positions to the ship based on data streams provided by R. Leben. J. Hummon processed the ship's acoustic Doppler current profiler data. We thank D. Capone, E. Carpenter, J. Waterbury, P. Falkowski, S. Dyhrman, E. Webb, and two anonymous reviewers for their helpful comments on this paper. Funding for development of the VPR was provided by a NSF Ocean Technology and Interdisciplinary Coordination grant OCE-9820099. Further support for VPR testing and operations was provided by NSF Oceanographic Technical Services grant OCE-0308366 and from the J. Seward Johnson Endowment Fund, the Penzance Foundation, and WHOI Biology Department Discretionary Funds. C.S.D. was supported by the Richard B. Sellars Endowed Research Fund, the Andrew W. Mellon Foundation Endowed Fund for Innovative Research, and a fellowship from WHOI's Ocean Life Institute. D.J.M. was supported by NSF grant OCE-0241310 and NASA grant NNG04GR22G.

Supporting Online Material

www.sciencemag.org/cgi/content/full/312/5779/1517/DC1
Materials and Methods
Figs. S1 to S3
Table S1
References and Notes

7 December 2005; accepted 13 April 2006
10.1126/science.1123570

TOPLESS Regulates Apical Embryonic Fate in *Arabidopsis*

Jeff A. Long,[1]* Carolyn Ohno,[2] Zachery R. Smith,[1] Elliot M. Meyerowitz[2]

The embryos of seed plants develop with an apical shoot pole and a basal root pole. In *Arabidopsis*, the *topless-1* (*tpl-1*) mutation transforms the shoot pole into a second root pole. Here, we show that TPL resembles known transcriptional corepressors and that *tpl-1* acts as a dominant negative mutation for multiple TPL-related proteins. Mutations in the putative coactivator *HISTONE ACETYLTRANSFERASE GNAT SUPERFAMILY1* suppress the *tpl-1* phenotype. Mutations in *HISTONE DEACETYLASE19*, a putative corepressor, increase the penetrance of *tpl-1* and display similar apical defects. These data point to a transcriptional repression mechanism that prevents root formation in the shoot pole during *Arabidopsis* embryogenesis.

The apical/basal axis of *Arabidopsis* embryos is established during the first cell division of the zygote, and auxin accumulation and response have been shown to be important for early steps in axis establishment (*1*–*5*). As the embryo matures, specific cell types become apparent, and a clear shoot/root axis is visible at the transition stage of development (*6*, *7*). Although several mutants have been isolated that affect the formation of specific patterning elements of the shoot at the transition stage of embryogenesis, only *topless-1* (*tpl-1*) so far switches the identity of the shoot into that of a root (*8*–*11*). It is therefore likely that *TPL* is acting at a different level of control than those factors that have previously been isolated.

tpl-1 mutants are temperature sensitive and at the restrictive temperature (29°C) transform the embryonic shoot pole into a second root pole that gives rise to a double-root seedling (*11*) (Fig. 1, A and B). At lower temperatures, *tpl-1*embryos fail to form a shoot apical meristem and show varying degrees of cotyledon fusion (Fig. 1, C to E). We view these phenotypes as a result of partial apical-to-basal transformation during embryogenesis (*11*) (fig. S1). Previous work has shown that transition-stage *tpl-1* embryos lack or have reduced expression of genes associated with the apical half of the embryo, whereas the expression patterns of genes associated with the basal half of the embryo are expanded into the apical half and are ultimately duplicated. Pre–transition stage *tpl-1* embryos are morphologically indistinguishable from those of the wild type.

To examine the molecular organization of the apical half of *tpl-1* pre–transition stage embryos, we performed in situ hybridizations with the transcription factor *WUSCHEL* (*WUS*) (*10*). *WUS* is initially expressed in a small group of cells in the apical half of 16-cell-stage embryos. *WUS* mRNA accumulated normally in *tpl-1* globular-stage embryos, but was absent in transition-stage embryos at 29°C (Fig. 1, F to H). This indicates that early *tpl-1* embryos have established an apical axis with the correct organization, but this fate is lost or masked at the transition stage.

tpl-1 was mapped to bacterial artificial chromosome F7H2 on chromosome 1 using polymerase chain reaction–based markers (*11*). We found two base-pair substitutions in At1g15750 (*12*) that cosegregated with the *tpl-1* phenotype and result in a change of a lysine (K) to a methionine (M) at amino acid 92 and an asparagine (N) to a histidine (H) at amino acid 176 of the predicted protein (*13*). Concurrently, we conducted a high-temperature ethylmethane sulfonate suppressor screen in the *tpl-1* background and found five semidominant suppressors that mapped to the original *TPL* locus. We sequenced At1g15750 from these lines and found that each harbored a second site mutation that is

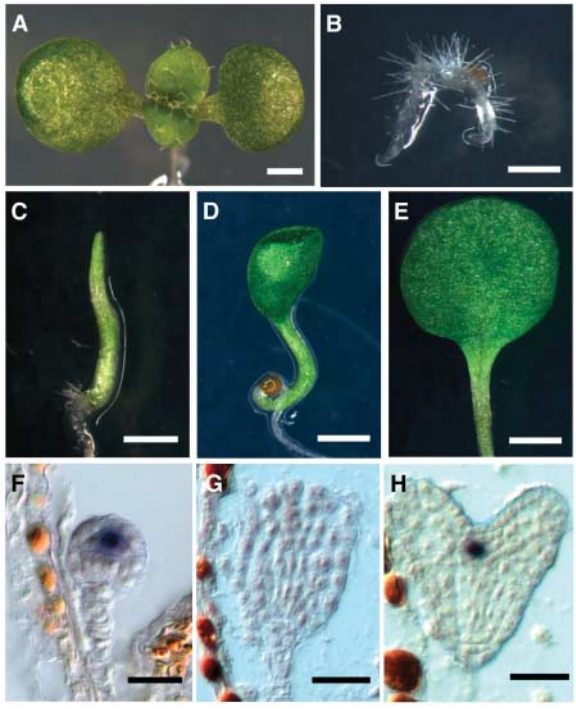

Fig. 1. Effects of *topless-1* on embryonic polarity. (**A**) Wild-type 5-day-old seedling. (**B**) A *tpl-1* double-root seedling. (**C**) A *tpl-1* pin seedling lacking cotyledons. (**D**) A *tpl-1* tube seedling. (**E**) A *tpl-1* monocot seedling with two fused cotyledons. (**F**) *WUS* mRNA accumulation in a *tpl-1* globular-stage embryo grown at 29°C. (**G**) *WUS* mRNA does not accumulate in a *tpl-1* heart-stage embryo. (**H**) Wild-type heart-stage embryo accumulating *WUS* mRNA in a small group of cells in the developing meristem. Scale bars: 1 mm (A to E), 25 μm (F to H).

[1]Plant Biology Laboratory, The Salk Institute for Biological Sciences, 10010 North Torrey Pines Road, La Jolla, CA 92037, USA. [2]Division of Biology, California Institute of Technology, 1200 East California Boulevard, Pasadena, CA 91125, USA.

*To whom correspondence should be addressed. E-mail: long@salk.edu